JOURNAL OF GUIDANCE, CONTROL, AND DYNAMICS
Vol. 15, No. 4, July-August 1992

Comparison of Two Dissimilar Modal Identification Techniques

Richard S. Pappa*
NASA Langley Research Center, Hampton, Virginia 23665
and
Axel Schenk,† Norbert Niedbal,† and Erhard Klusowski†
German Aerospace Research Establishment (DLR), Göttingen, W-3400 Germany

Recent laboratory results using a refined phase resonance method and the eigensystem realization algorithm on the same test structure are reported. These methods are dissimilar modal identification techniques suitable for future large spacecraft. The theory, application approach, and results obtained for each technique are summarized and compared. Although both methods worked well in this investigation, significant differences occurred in some identified mode shapes. Comparison of independently derived modal parameters provides the means for disclosing such discrepancies in flight projects.

Introduction

THE on-orbit dynamic characteristics of future large space structures, such as Space Station Freedom, can significantly affect mission performance. Unexpected vibration can disrupt microgravity experiments, remote-sensing measurements, and the operation of control systems. Furthermore, multiple payloads can interact through flexible adjoining structure. Modal identification tests are required for verification of the predicted dynamic characteristics. Because of their size and complexity, these structures pose unprecedented challenges to modal testing technology.[1,2] Improvement and elaboration of current methods are necessary.

In the classical phase resonance method (PRM) of modal testing,[3-6] each normal mode of vibration is excited individually using multiple shakers with appropriated, sinusoidal forces. Modern implementations consider all responses simultaneously to optimize modal purity indicated by the phase resonance criterion. Real-time displays provide direct observation of mode shapes and mode indicator functions. Recent refinements include new data condensation methods and improved estimates for optimal excitation.[6]

In an entirely different approach to modal testing, modal parameters are derived from multiple-mode response data with computer algorithms. A method known as the eigensystem realization algorithm (ERA) has been developed for multiple-input/multiple-output analysis of frequency response or free decay data.[7-10] With this approach, a reduced state-space model suitable for control synthesis is also available. Recent refinements include methods for improving results using emphasized data[9] and a consistent-mode indicator function.[10]

This paper discusses a research application of these two dissimilar modal identification techniques. Both techniques are candidate approaches for future large spacecraft. The theory, application approach, and results obtained for each method are summarized and compared.

Received July 26, 1991; revision received Nov. 12, 1991; accepted for publication Nov. 25, 1991.

*Aerospace Engineer, Spacecraft Dynamics Branch, Mail Stop 230.
†Aerospace Engineer, Institute of Aeroelasticity, Bunsenstraße 10.

Test Structure

The test article for this investigation is shown in Fig. 1. It consists of a cylindrical mast and four rectangular beams of various lengths. The beams are clamped at their centers to the tip and middle of the mast. The lower pair of beams is rotated 45 deg with respect to the upper pair. One beam of each pair contains a silicon layer at the neutral axis for additional damping. The overall dimensions are 1.59 m in height and 1.40 m in width, and the total mass is approximately 50 kg. The dynamic response of the structure was measured with 48 accelerometers.

This structure was designed to provide specific dynamic characteristics including modal clusters, local response behavior, and damping coupling. Furthermore, considerable nonlinearity was introduced by the silicon material. These properties are representative of realistic spacecraft characteristics.

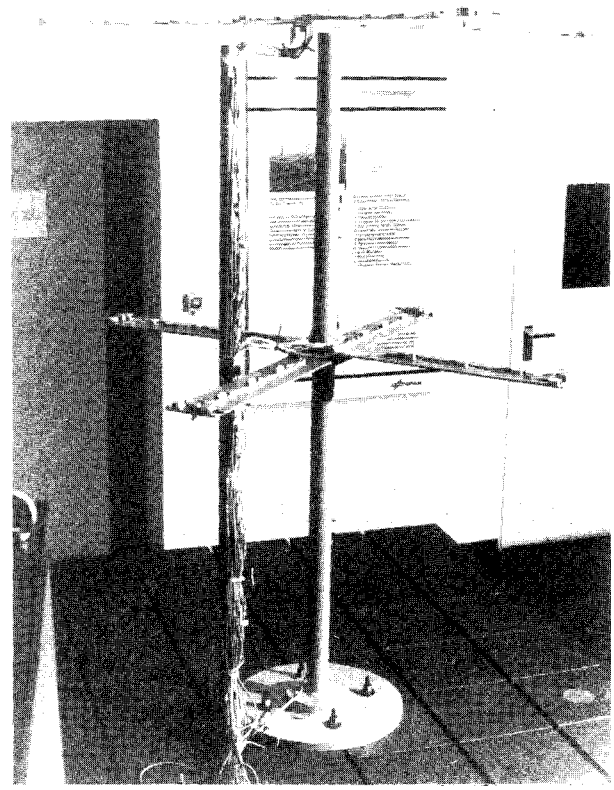

Fig. 1 Test structure.

Phase Resonance Method

Theory

The structural dynamic behavior of a linear elastomechanical system without gyroscopic effects is formulated by means of the generalized mass matrix $\boldsymbol{M}$, the generalized stiffness matrix $\boldsymbol{K}$, the generalized structural damping matrix $\boldsymbol{D}$, and the generalized exciter forces $\Phi^T\boldsymbol{F}$. Applying sinusoidal excitation forces with circular frequency ω, the generalized equation of motion reads:

$$(-\omega^2\boldsymbol{M}+j\boldsymbol{D}+\boldsymbol{K})\boldsymbol{q} = \Phi^T\boldsymbol{F} \tag{1}$$

The modal matrix Φ contains n_g normal modes with n_p physical measurement stations.

The dynamic response will also be sinusoidal but with a phase lag φ relative to the excitation. The generalized equation of motion can be separated into its real and imaginary parts:

$$(-\omega^2\boldsymbol{M}\cos\varphi+\boldsymbol{K}\cos\varphi-\boldsymbol{D}\sin\varphi)\boldsymbol{q} = \Phi^T\boldsymbol{F} \tag{2a}$$

$$(-\omega^2\boldsymbol{M}\sin\varphi+\boldsymbol{K}\sin\varphi+\boldsymbol{D}\cos\varphi)\boldsymbol{q} = 0 \tag{2b}$$

A phase shift of $\varphi = 90$ deg between the exciter forces and the structural responses yields

$$-\boldsymbol{D}\boldsymbol{q} = \Phi^T\boldsymbol{F} \tag{3a}$$

$$(-\omega^2\boldsymbol{M}+\boldsymbol{K})\boldsymbol{q} = 0 \tag{3b}$$

Equations (3a) and (3b) define the phase resonance condition. The applied excitation energy must compensate for the structural damping energy, Eq. (3a). Also, the excitation frequency must equal the corresponding undamped natural frequency, Eq. (3b). A proven tool to fulfill these objectives is the mode indicator function,[3] also known as the phase resonance criterion (PRC):

$$\mathrm{PRC} = \left[1.0 - \frac{\sum_{i=1}^{np} |y_i'||y_i|}{\sum_{i=1}^{np} |y_i|^2}\right] \cdot 1000 \tag{4}$$

where y_i' and $|y_i|$ are the real part and magnitude, respectively, of the ith response measurement with respect to the applied force.

The unknown internal damping distribution must be compensated by external exciter forces. The force appropriation procedures of Traill-Nash,[11] Asher,[12] and Ibáñez[13] are only based on the real-part formulation, which is tuned to become zero. These methods interpret the real parts as parasitic contributions of the neighboring normal modes. Other methods[14,15] only consider the imaginary parts of the structural responses. Here, the imaginary parts are minimized by canceling the input energy of neighboring modes:

$$\tilde{\Phi}''^T\boldsymbol{F}_r = \begin{bmatrix} 0 \\ 0 \\ 1 \\ 0 \\ 0 \end{bmatrix} \tag{5}$$

Consequently, the procedures of Hunt et al.[16] and Niedbal and Klusowski[6] consider both real and imaginary parts simultaneously and achieve the most reliable and robust results; however, they require additional measurements. In this project, the Anderson approach was considered to be sufficient. It was the only approach used.

Adequate positioning of a sufficient number of exciters is also required. The necessary number of exciter forces is defined by Eq. (5); that is, the number of forces must equal the number of normal modes considered. Exciter placement is solved using combinatorial optimization by locating the $n_g \cdot n_g$ submatrix $\tilde{\Phi}''$ with the highest condition number.[6]

Application Approach

Figure 2 summarizes the PRM procedure. Each normal mode is excited individually using multiple shakers with sinusoidal excitation at the natural frequency. If necessary, iteration is used to achieve adequate mode purity.

To create an a priori data base for optimal exciter point selection and force tuning, 10 sweep runs were performed. Four symmetrical and four antisymmetrical pairs of exciter forces were applied at the tips of each cantilever beam. Two additional horizontal force configurations excited the bending and torsional modes of the mast. Typical results are shown in Fig. 3. Peaks in the mode indicator function, Eq. (4), indicate modes of vibration. Among the 10 sweep runs, a total of 111 peaks are identified from 0 to 100 Hz. Comparing the individual response deformations by means of a difference criterion,[6] 26 independent deformation vectors are found.

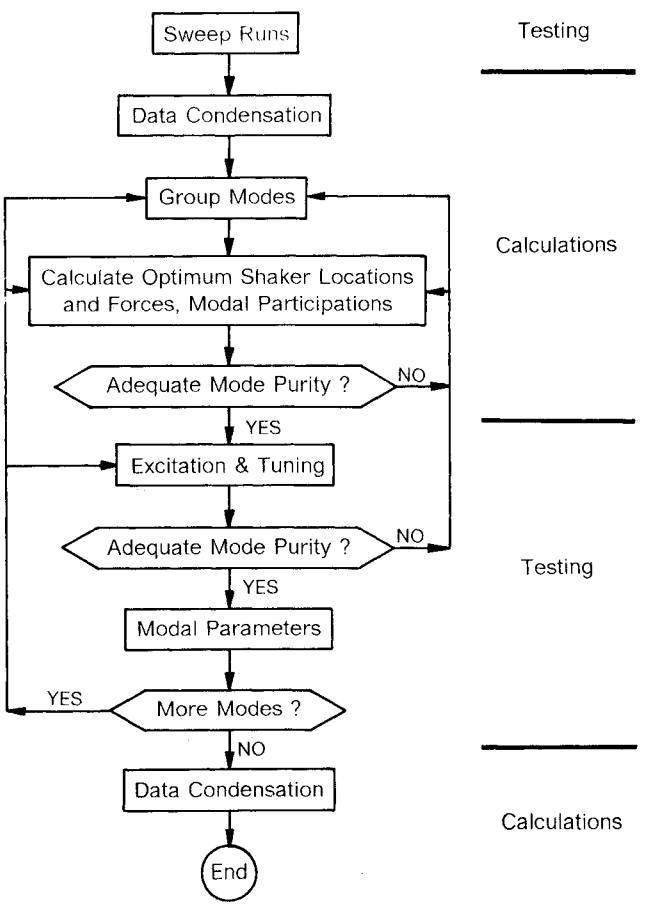

Fig. 2 PRM flowchart.

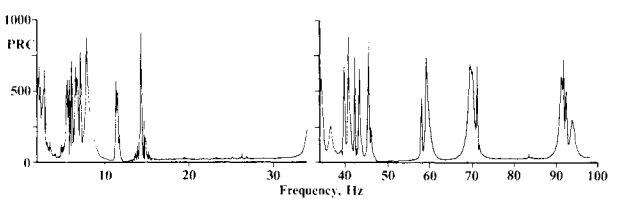

Fig. 3 Sweep run.

Using this information, optimal exciter points are selected based on the $n_g \cdot n_g$ modal submatrix having the highest condition number. In most cases, three or four normal modes were combined in one group; that is, three or four shakers were applied. Most exciter points were selected at the tips of the cantilever beams in either the horizontal or vertical directions. Only a few modes required excitation at the mast tip and/or in the middle of the mast. Force vectors were determined according to Eq. (5). A final tuning of phase purity was performed by hand, considering that the exciter point selection and force determination are based on estimates of the normal modes only. The exciter point selections were not changed during the final tuning.

Real-time displays of the 48 accelerometer signals (both real and imaginary parts) and the mode indicator function were available to the test operators. These data greatly facilitated mode tuning and optimization of PRC.

Results

Table 1 shows the natural frequency, damping factor (equivalent viscous damping), and PRC results obtained for each normal mode below 100 Hz. All indicator values are approximately 950 or higher, indicating excellent modal purity. During testing, modes were considered to be adequately tuned once a value of approximately 950 was achieved. There is little practical difference between a PRC value of 950 and a perfect result of 1000.

The damping results shown in Table 1 are averaged values based on four different estimates.[17] The individual values are presented later in comparison with ERA results. The identified natural frequencies are assumed to be accurate to within 1% for the test conditions under which they were obtained and are not discussed further.

A typical identified mode shape is shown in Fig. 4. Magnitude and phase results are plotted vs measurement number. The measurements are arranged sequentially along the four cantilever beams, the lateral tip locations, and the mast. This mode has an indicator value of 974. Thus, the majority of mode-shape components have phase angles of approximately ±90 deg—characteristic of a classical normal mode. Exceptions are measurements 1-8, 28, and 45-48. Measurements 1-8 are located on one of the damped cantilever beams. Since silicon was applied to only two structural members, the damping distribution is nonproportional to the mass and/or stiffness distribution, resulting in damping coupling (complex modes). The phase angle errors for beam 1 are attributed to these effects. The results could be improved using additional exciters. This was not done during testing, however, because of the relatively high modal purity already achieved. Phase angle errors for measurements 28 and 45-48 are meaningless because the corresponding magnitudes are approximately zero.

Table 1 Phase resonance method results [a,b]

Mode	Frequency, Hz	Damping factor, %	Phase resonance criterion
1	5.375	2.109	972
2	5.757	0.484	974
3	6.536	3.410	936
4	6.628	1.871	991
5	6.793	2.699	942
6	7.193	1.552	958
7	7.705	2.297	983
8	8.524	4.986	990
9	11.121	1.203	993
10	11.236	0.960	986
11	14.200	0.252	995
12	34.310	1.580	976
13	36.417	1.725	973
14	38.820	0.222	986
15	40.857	0.382	969
16	41.368	0.284	988
17	42.467	1.034	986
18	43.507	0.383	958
19	44.767	1.836	953
20	45.654	0.285	978
21	56.743	0.416	957
22	57.980	0.435	974
23	71.371	0.650	944
24	72.231	0.355	971
25	91.906	1.056	968
26	93.385	0.937	933

[a] 22 of 26 modes with PRC>950.
[b] 0 of 26 modes with PRC<900.

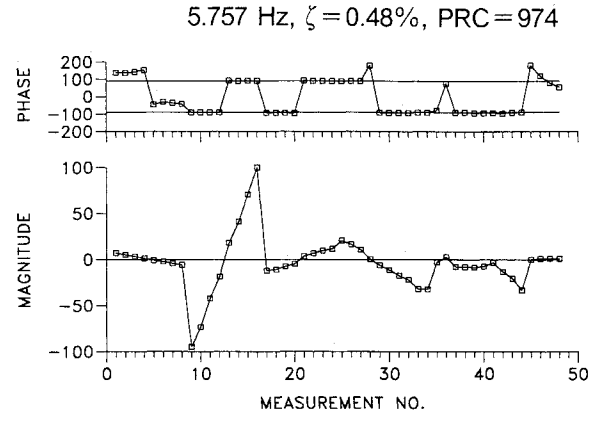

Fig. 4 PRM mode 2.

Eigensystem Realization Algorithm

Theory

A finite-dimensional, linear, time-invariant dynamic system can be represented by the state-variable equations:

$$\dot{x}(t) = A_c x(t) + Bu(t) \tag{6a}$$

$$y(t) = Cx(t) \tag{6b}$$

where x is an n-dimensional state vector, u a p-dimensional excitation vector, and y a q-dimensional response vector. The matrix A_c characterizes the dynamics of the system, and B and C relate the internal state variables x to the external excitation and response vectors u and y.

A special solution to Eqs. (6a) and (6b) is the impulse response function:

$$Y(t) = Ce^{A_c t}B \tag{7}$$

for $t \geq 0$. The ith column of $Y(t)$ contains the free response of the system, with $x(0) = 0$, to a unit-impulse excitation applied at the ith input location at $t = 0$. With sampled data, this solution can be expressed as

$$Y(k) = CA^k B \tag{8}$$

for $k \geq 0$. $A = e^{A_c \Delta t}$ is the state-transition matrix, and Δt is the data sampling interval.

The problem of system realization is as follows: Given a sequence of experimentally measured $Y(k)$, for $k = 0,1,2,\ldots$, construct a triplet $[A,B,C]$ such that Eq. (8) is satisfied. Experimental response data for multiple excitation locations (or initial conditions) are typically used simultaneously to permit efficient identification of closely spaced modes. Note that $[A,B,C]$ is not unique since the set $[T^{-1}AT, T^{-1}B, CT]$, for any nonsingular matrix T, also satisfies the state-variable equations.

The ERA solution to the system realization problem uses singular-value decomposition of the generalized Hankel matrix:

$$H(0) = U\Sigma V^T \tag{9}$$

The matrix $H(0)$ consists of time-shifted $Y(k)$ submatrices.[7,8] The diagonal matrix Σ contains the ordered singular values of $H(0)$, and U and V contain the corresponding left and right singular vectors, respectively.

Retaining the n largest singular values, an nth-order realization is computed as

$$A = \Sigma_n^{-1/2} U_n^T H(1) V_n \Sigma_n^{-1/2} \tag{10a}$$

$$B = \Sigma_n^{1/2} V_n^T E_p \tag{10b}$$

$$C = E_q^T U_n \Sigma_n^{1/2} \tag{10c}$$

where $H(1)$ is a second generalized Hankel matrix shifted in time by one data sample from $H(0)$. E_p and E_q are pth-order and qth-order selector matrices.

The realization given in Eqs. (10a-10c) is transformed to modal coordinates using the eigenvalues Z and eigenvector matrix Ψ of A as follows:

$$A' = \Psi^{-1} A \Psi = Z \tag{11a}$$

$$B' = \Psi^{-1} B \tag{11b}$$

$$C' = C\Psi \tag{11c}$$

The modal damping rates σ_i and the damped natural frequencies ω_i are the real and imaginary parts of the continuous-domain eigenvalues:

$$s_i = \sigma_i \pm j\omega_i = \ell n(z_i)/\Delta t \tag{12}$$

Modal participation factors and mode shapes are the corresponding rows of B' and columns of C', respectively.

In practice, not all eigenvalues and eigenvectors obtained using this approach are valid structural modes due to noise, nonlinearity, uncertainty concerning the number of modes present, etc. Several indicators are available to establish the relative accuracy of the various results.[7,8,10]

The phase resonance criterion, Eq. (4), is also computed for every identified mode. Each (complex) mode shape is rotated so that the phase angles align best with ±90 deg, and then Eq. (4) is applied.

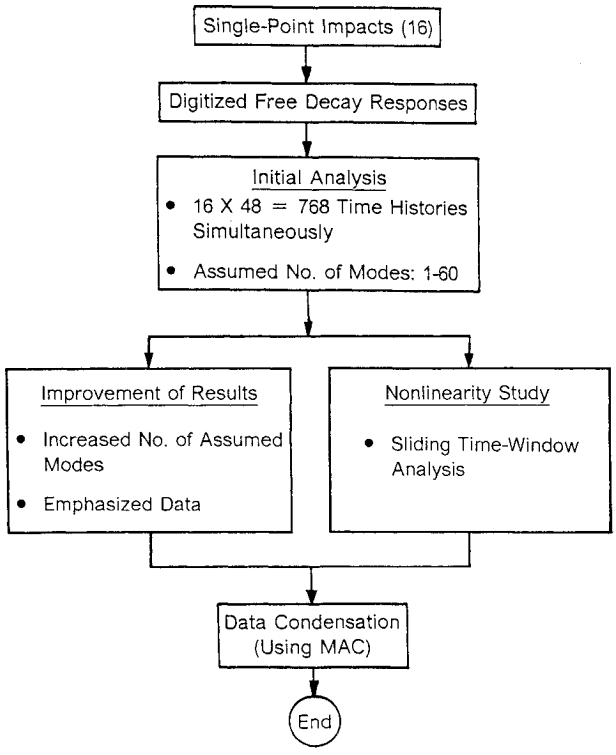

Fig. 5 ERA flowchart.

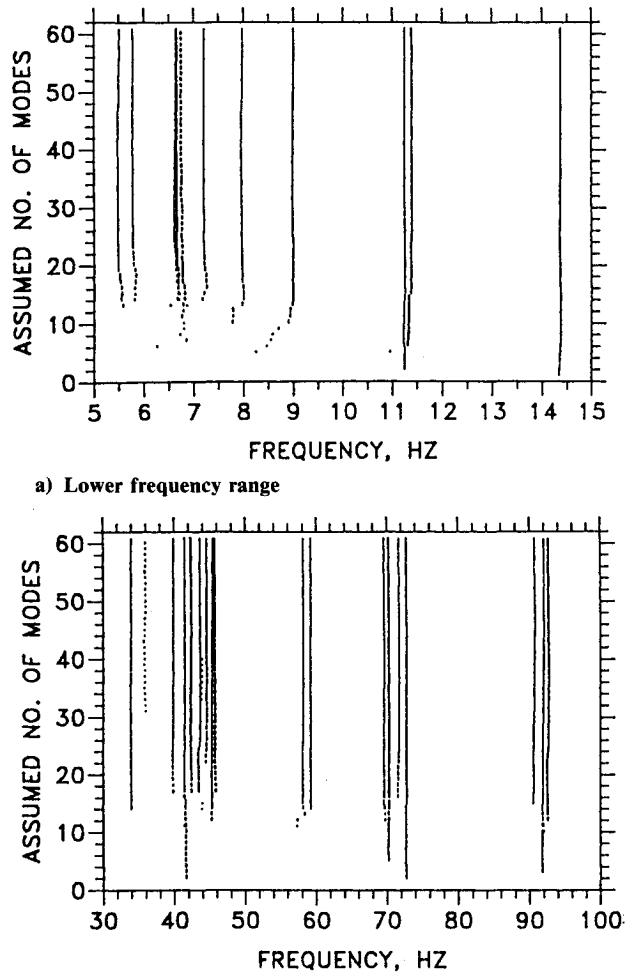

Fig. 6 Initial analysis.

Application Approach

Figure 5 summarizes the ERA procedure. Modal identification was performed using directly measured free-decay data. The structure was excited using a rubber-tipped hammer. To ensure excitation of all modes from 0 to 100 Hz, 16 separate single-point impacts were applied: four on the upper beams, four on the lower beams, four on the mast, and four in torsion. A force measurement triggered the data acquisition process. Each measurement period was 5.12 s long with a sampling frequency of 400 Hz.

Three types of data analysis were performed: an initial overview analysis, additional analyses for improving specific results, and a nonlinearity study. Each of the three data-analysis steps are discussed separately in the following sections.

Results

Initial Analysis

An initial analysis was performed using all response measurements ($16 \times 48 = 768$ time histories) simultaneously. The data were digitally filtered into two frequency bands: 0–25 and 20–100 Hz. Each filtered data set was analyzed separately. A generalized Hankel matrix of 160 columns and 960 rows was constructed. Default values for all other analysis parameters were used. These choices resulted in the use of 0.94 s of data in the 0–25-Hz range and 0.27 s of data in the 20–100-Hz range.

Previous experience has shown that significant changes in the identified parameters can occur as a function of the as-

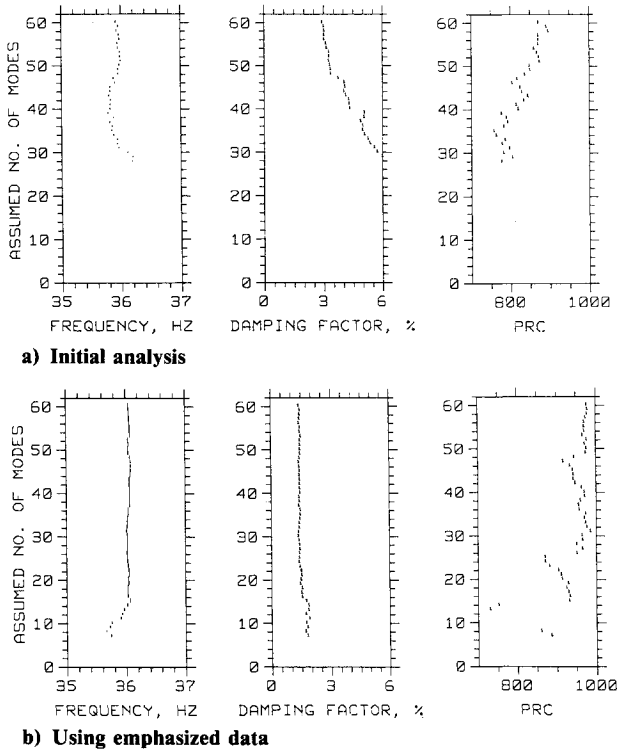

Fig. 7 Improvement of results.

sumed number of modes.[9] In particular, optimum accuracy for different modes typically occurs at different numbers of assumed modes. Also, weakly excited modes often require relatively high numbers of assumed modes to be properly identified. For these reasons, the assumed number of modes was incremented in each analysis from 1 to 60.

The identified natural frequencies are shown in Fig. 6. Each row of results corresponds to a separate analysis with a specified number of assumed modes. Each detected mode is represented by a vertical dash at the associated frequency. The confidence in each result is expressed by the length of the vertical dash, which is proportional to the accuracy indicator known as the consistent-mode indicator (CMI).[9,10] CMI measures the consistency of mode-shape components, both temporally and spatially. Components from the beginning of the data analysis window are compared with corresponding components at the end of the window. The spatial collinearity of mode-shape phase angles is also included in the calculation. In Fig. 6, the highest confidence is attained if the distance between minor tic marks on the vertical axis is filled. Thus, more confidence is associated with results appearing as solid vertical lines than with those appearing as dotted or dashed lines.

Overall, 30 modes are found in the frequency range from 0 to 100 Hz. With two exceptions at approximately 6.7 and 36 Hz, all modes are identified as straight and solid lines with increasing numbers of assumed modes, indicating consistency and reliability.

Improvement of Results

Of the 30 modes in the initial analysis, 23 had PRC values greater than 950. However, certain results are unsatisfactory. Two independent methods are described in this section for improving the results. In contrast to the on-line and real-time approach of the PRM off-line methods such as ERA offer various possibilities for post-test improvement of results.

In the initial analysis, CMI increased for most modes over the entire range of assumed modes. Therefore, additional single analyses were performed using larger identification orders. For research purposes, it is interesting to investigate the effect of increasing the number of assumed modes to extreme values as well as enlarging the data matrix size and consequently extending the analysis time window. With linear structures, longer data lengths increase modal identification accuracy (until the modal response level decays below the noise floor). With nonlinearities, however, identification accuracy can deteriorate with longer data lengths due to changing modal parameters as a function of response level.

Three additional analyses were performed using 80, 100, and 160 assumed modes. Compared with the initial results, 25 of 30 modes now have indicator values above 950. In particular, mode purity increased for 19 modes. Six modes exhibited nearly perfect mode purity with PRC values greater than 990.

For the first time, a new approach for improving results using emphasized data was applied in this project. The technique is based on the fact that noisy response measurements (for particular modes) deteriorate the proper identification of modal parameters. Improvement is possible if information about optimal excitation and response locations is available. Such information is provided by ERA's accuracy indicators.

The success of this technique is illustrated in Fig. 7. Figure 7a provides an expanded view of the initial analysis in a narrow range near 36 Hz. Corresponding damping and indicator values are also shown. The results are relatively unsatisfactory, indicated by low CMI (lengths of the dashes in the frequency plot), PRC values below 900, and an unstable and curved pattern of damping estimates over the entire range of assumed modes. Corresponding results using emphasized data with optimal excitation and sensing are shown in Fig. 7b. Stable and reliable identification of frequency and damping over nearly the entire range of assumed modes is obtained. Indicator values of up to 986 indicate a much improved mode shape identification.

In summary, this new technique provided significant improvement of results for several modes that were weakly identified in the initial analysis. The technique used the initial-analysis results to select optimal excitation and response points. Each mode of interest was improved in a dedicated analysis.

Nonlinearity Study

Nonlinearities were investigated using a sliding time-window analysis. Forty separate analyses were performed using a starting time varying from 0.0 to 4.0 s. Each analysis used the same parameters as before, with 60 assumed modes.

Significant changes in identified natural frequencies occurred as a function of response amplitude for modes associated with the damped beams. A typical result is shown in Fig. 8. Mode 3 involves symmetric bending of the undamped upper beam. Its frequency is constant as a function of time shift (lower amplitudes occur at larger time shifts). The frequencies of modes 4 and 5, on the other hand, increase considerably. These modes involve symmetric bending of the damp-

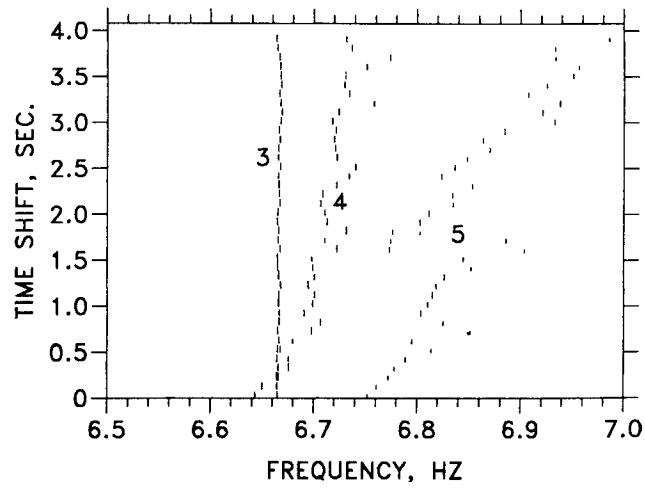

Fig. 8 Nonlinearity study.

ing upper beam. They are also highly coupled with mast bending. In mode 4, the two halves of the beam move in phase with the mast, whereas in mode 5, they move out of phase. Nonlinearities combine with significant damping coupling to complicate reliable identification of these modes.

Summary of Best Results

The best results from all analyses, based on the phase resonance criterion, are taken as the final modal parameters. These values are listed in Table 2. Excellent results were obtained, with 29 of 30 modes having PRC values above 950. The unusually low indicator value for mode 5 is attributed to damping coupling and nonlinearity caused by the silicon material.

Comparison of Results

A common method for correlating pairs of experimental mode-shape vectors Φ_i and Φ_j is the modal assurance criterion (MAC),[18] defined as

$$\mathrm{MAC}_{ij} = \frac{|\Phi_i^H \Phi_j|^2}{(\Phi_i^H \Phi_i)(\Phi_j^H \Phi_j)} \tag{13}$$

where H designates the Hermitian transpose. Values greater than approximately 0.7 indicate a significant degree of similarity.

Using this approach, the 26 modes listed in Table 1 are correlated with the 30 modes listed in Table 2. These results are presented in Fig. 9 using a simple graphical format. Each row and column represents one mode shape. The value of MAC is proportional to the size of the rectangle drawn at the intersection of the corresponding row and column. Values greater than 0.7 are darkened for emphasis.

Figure 9 shows an excellent, one-to-one correspondence of results. The only irregularities observed are two instances of mode-ordering differences—attributed to small frequency shifts due to nonlinearities—and the absence of corresponding

Table 2 Eigensystem realization algorithm results[a,b]

Mode	Frequency, Hz	Damping factor, %	Phase resonance criterion
1	5.501	1.421	989
2	5.780	0.237	989
3	6.664	0.130	995
4	6.686	1.451	955
5	6.774	1.163	818
6	7.211	0.316	985
7	7.978	1.306	984
8	9.005	1.767	994
9	11.251	0.095	994
10	11.391	0.089	997
11	14.370	0.057	995
12	33.989	1.627	990
13	36.012	1.354	986
14	39.901	0.067	996
15	41.520	0.189	994
16	42.377	0.077	997
17	43.596	0.178	974
18	44.575	1.162	982
19	45.428	1.348	983
20	45.680	0.159	965
21	58.141	0.349	994
22	59.179	0.390	994
23	69.623	0.518	958
24	70.304	0.405	977
25	71.693	0.131	990
26	72.736	0.134	995
27	90.776	0.883	984
28	91.964	0.098	963
29	92.257	0.808	969
30	92.647	0.246	969

[a] 29 of 30 modes with PRC > 950.
[b] 1 of 30 modes with PRC < 900.

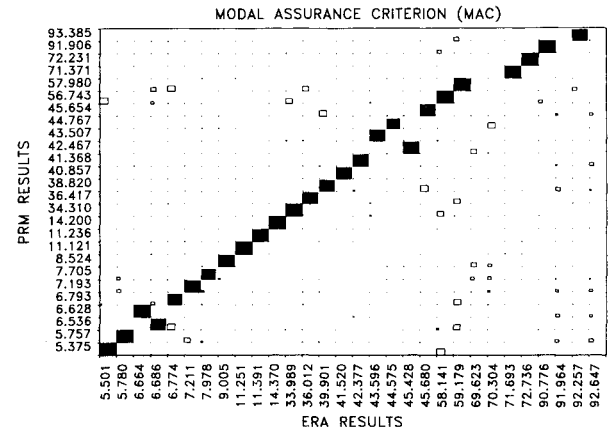

Fig. 9 Mode-shape correlation.

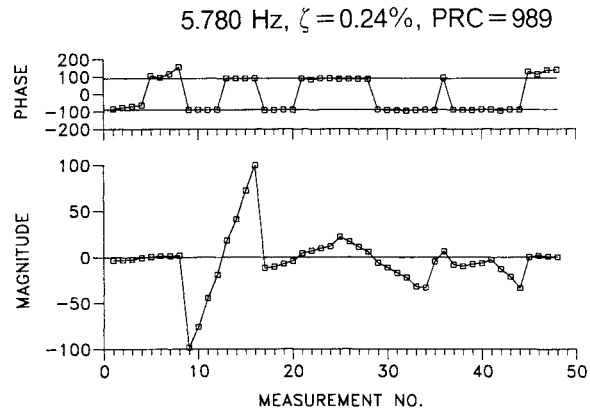

Fig. 10 ERA mode 2.

PRM results for four ERA modes at high frequencies. These four modes, at approximately 70 and 90 Hz, are fundamental torsional modes of the cantilever beams. They were only weakly observed in the tests because accelerometers were located on the centerlines of the beams (except at the tips, where they were slightly offset). Furthermore, excitation was also applied only along the centerlines. These modes were apparently excited better by accident in the ERA tests because of small deviations in the impact locations.

Modes with high modal assurance criterion values are often considered to be identical for all practical purposes. This is a good assumption if the mode-shape differences are random errors. In this investigation, however, some instances of deterministic errors were observed among the various mode pairs. An example is mode 2. The phase resonance result was shown previously in Fig. 4. The corresponding ERA result is plotted in Fig. 10. These two mode shapes are essentially identical for measurements 9–48. The correlation coefficient is thus very high—99%. However, the motion of beam 1 (measurements 1–8) in Fig. 4 is 180 deg out of phase with that in Fig. 10. Such polarity errors can cause instabilities to occur if these system identification results are used for control design purposes. Each result was considered to be correct based on all indicators available with the individual methods. This discrepancy was detected only by a close comparison of the independently derived results.

The final comparison performed is with the identified damping values. Viscous damping factors determined by both methods are shown in Fig. 11. Modes involving the damped cantilever beams show values above approximately 1%, whereas the remaining modes show values lower than approximately 0.5%. Considering the large scatter of results seen in other test comparisons, for example by Chen,[19] the results presented here show an overall good correlation. The general trend of the ERA values to be smaller than correspond-

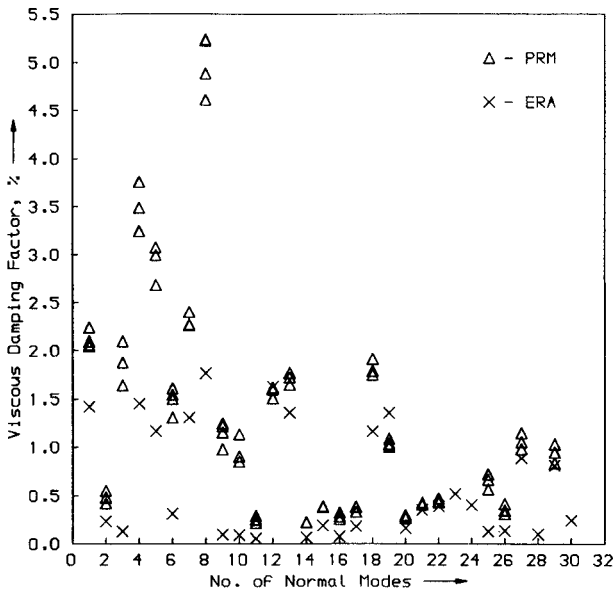

Fig. 11 Damping comparison.

ing PRM results is attributed to lower response levels with impact excitation than with sinusoidal, resonant excitation. A small additional damping force may have also been introduced by the attached shakers in the phase resonance tests.

Conclusions

In this application, the natural frequencies and mode shapes determined using the phase resonance method and the eigensystem realization algorithm are mostly identical within engineering accuracy. The majority of mode pairs correlated with a modal assurance criterion greater than 90%. Identified damping values, on the other hand, showed larger differences. Although mode indicator values were greater than 950 for most modes with both techniques, the majority of values (22 of 26 common modes) were higher using the eigensystem realization algorithm. Phase purity for several modes was improved substantially in this approach using larger numbers of assumed modes and a new method for selecting emphasized data. With the phase resonance method, mode tuning was generally stopped once a value of approximately 950 was achieved.

Both techniques discussed in this paper are considered to be feasible approaches for modal identification of future large spacecraft. The similarity of results validates the accuracy of each method. However, significant differences occurred in some identified mode shapes. Comparison of independently derived modal parameters provides the means for disclosing such discrepancies in flight projects.

Acknowledgment

This work was performed under a collaborative research agreement between NASA and the German Aerospace Research Establishment in the area of dynamics and control of large space systems.

References

[1]Hornung, E., Breitbach, E., and Öry, H., "Recent Developments and Future Trends in Structural Dynamic Design Verification and Qualification of Large Flexible Spacecraft," *Proceedings of the NATO AGARD Conference,* Oberammergau, Germany, Sept. 9–13, 1985.

[2]Pappa, R. S., "Identification Challenges for Large Space Structures," *Sound and Vibration,* April 1990, pp. 16–21.

[3]Breitbach, E., "A Semi-Automatic Modal Survey Test Technique for Complex Aircraft and Spacecraft Structures," *Proceedings of the 3rd ESRO Testing Symposium,* Frascati, Italy, Oct. 1973, pp. 519–528.

[4]Niedbal, N., and Hüners, H., "Modal-Survey Testing for System Identification and Dynamic Qualification of Spacecraft Structures," *Proceedings of the NATO AGARD Conference,* Oberammergau, Germany, Sept. 9–13, 1985.

[5]Degener, M., and Hüners, H., "Experiences With and Prospects for Dynamic Mechanical Testing of Spacecraft Structures," European Space Agency SP-304, June 1990, pp. 309–315.

[6]Niedbal, N., and Klusowski, E., "Optimal Exciter Placement and Force Vector Tuning Required for Experimental Modal Analysis," AIAA Paper 90-1205, April 1990.

[7]Juang, J.-N., and Pappa, R. S., "An Eigensystem Realization Algorithm for Modal Parameter Identification and Model Reduction," *Journal of Guidance, Control, and Dynamics,* Vol. 8, No. 5, 1985, pp. 620–627.

[8]Juang, J.-N., and Pappa, R. S., "Effects of Noise on Modal Parameters Identified by the Eigensystem Realization Algorithm," *Journal of Guidance, Control, and Dynamics,* Vol. 9, No. 3, 1986, pp. 294–303.

[9]Pappa, R. S., Schenk, A., and Noll, C., "Eigensystem Realization Algorithm Modal Identification Experiences With Mini-Mast," NASA TM 4307, Feb. 1992.

[10]Pappa, R. S., "A Consistent-Mode Indicator for Eigensystem Realization Algorithm," *Proceedings of the AIAA Dynamics Specialists Conference,* AIAA Paper 92-2136, Dallas, TX, April 1992.

[11]Traill-Nash, R. W., "On the Excitation of Pure Natural Modes in Aircraft Resonance Testing," *Journal of the Aerospace Sciences,* Vol. 25, No. 12, Dec. 1958, pp. 775–778.

[12]Asher, G. W., "A Method of Normal Mode Excitation Utilizing Admittance Measurements," *Proceedings of the National Specialists Meeting on Dynamics and Aeroelasticity,* Nov. 1958, pp. 69–76.

[13]Ibáñez, P., "Force Appropriation by Extended Asher's Method," Society of Automotive Engineers, Paper 760873, Nov. 1976.

[14]Morosow, G., and Ayre, R. S., "Force Apportioning for Modal Vibration Testing Using Incomplete Excitation," *Shock and Vibration Bulletin,* No. 48, Pt. 1, Sept. 1978, pp. 39–48.

[15]Anderson, J. E., "Another Look at Sine-Dwell Mode Testing," *Journal of Guidance, Control, and Dynamics,* Vol. 5, No. 4, 1982, pp. 358–365.

[16]Hunt, D., Vold, H., Peterson, E., and Williams, R., "Optimal Selection of Excitation Methods for Enhanced Modal Testing," AIAA Paper 84-1068, May 1984.

[17]Niedbal, N., and Klusowski, E., "Die Ermittlung der generalisierten Masse and des globalen Dämpfungsbeiwertes im Standschwingungsversuch," *Journal of Flight Sciences and Space Research,* Vol. 13, 1989, pp. 91–100.

[18]Allemang, R. J., and Brown, D. L., "A Correlation Coefficient for Modal Vector Analysis," *Proceedings of the 1st International Modal Analysis Conference,* Union College, Schenectady, NY, Nov. 1982, pp. 110–116.

[19]Chen, J.-C., "Evaluation of Spacecraft Modal Test Methods," *Journal of Spacecraft and Rockets,* Vol. 24, No. 1, 1987, pp. 52–62.